doi: 10.4149/gpb_2024009

KRAS depletion suppresses ferroptosis and affects Hippo pathway in cataract

Hongda Jiang[1], Yinggui Yu[2] and Yu Yan[2]

[1] *Department of Laboratory Medicine, The Affiliated Hospital of Southwest Medical University, Luzhou City, Sichuan Province, China*
[2] *Department of Ophthalmology, The Affiliated Hospital of Southwest Medical University, Luzhou City, Sichuan Province, China*

Abstract. Cataract, a painless and progressive disorder is manifested as the opacification of the lens that represents the most significant cause of blindness worldwide. The objective of this study is to unveil the function of Kirsten rat sarcoma (KRAS) and potential action mechanisms against cataract. The ferroptosis-associated differentially expressed genes (DEGs) and pivot genes were extracted through the comprehensive bioinformatics methods. Erastin was applied for inducing ferroptosis in hydrogen peroxide (H_2O_2)-treated SRA01/04 cells, and validated by detecting content of intracellular iron, glutathione (GSH), malondialdehyde (MDA). Additionally, the effects of KRAS deficiency on ferroptosis were determined by functional assays. The proteins expression related to ferroptosis and Hippo pathway were determined by Western blotting. A total of 73 ferroptosis-related DEGs were discovered, and 6 critical core genes were confirmed upregulation in cataract cell model. The H_2O_2-treated SRA01/04 cells exhibited decrease of cell viability and proliferation, iron accumulation, MDA increase, GSH consumption, rise of COX2 and decline of GPX4, with further aggravated under erastin treatment, while the phenomena were improved by KRAS knockdown. Additionally, KRAS deficiency was involved in the Hippo signalling pathway activation. Downregulation of KRAS might restrain ferroptosis and affect Hippo pathway in cataract.

Key words: Cataract — KRAS — Ferroptosis — Hippo pathway — Bioinformatics

Introduction

Cataract, a painless and progressive disorder, is considered as the most significant cause of vision loss and impairment in the world that has affected approximately 95 million people (Liu et al. 2017; Lapp et al. 2023). It is estimated that blindness attributes to cataract in 15.2 million people over the age of 50, and the total number of cataract cases has increased by 29.7% throughout the last 20 years (GBD 2019 Blindness and Vision Inpairment Collaborators 2021). Although surgery is currently deemed as the most direct and effective therapy for treatment of cataracts, not all patients are able to receive surgery due to high cost (Lian et al. 2020; Xu et al. 2020). Furthermore, patients after surgery may suffer from several complications such as posterior capsule opacification, capsular rupture or vitreous loss, thus further limiting the availability of cataract surgery (Riaz et al. 2006). Therefore, it is still necessary to further clarify the complex pathogenesis underlying cataract, and explore more novel efficient targets for developing treatment strategies in cataract.

Ferroptosis, a distinct iron-dependent form is characterized by overwhelming accumulation of peroxidized lipids (Kim et al. 2023; Pope and Dixon 2023). Increasing

Electronic Supplementary material. The online version of this article (doi: 10.4149/gpb_2024009) contains Supplementary material.
Correspondence to: Yu Yan, No. 25, Tai Ping Street, Luzhou City, Sichuan Province, 646000, China
E-mail: yanyu19920@163.com

vast evidence has emerged indicating that ferroptosis may play a pivotal role in different physiological conditions and pathological processes, and it is implicated in the etiology of numerous diseases that collectively affect nearly every organ of the body, including ocular diseases (Liu et al. 2023; Wang et al. 2023). For instance, glaucoma with pathologically high intraocular pressure damage leads to elevated ferrous iron in the retina (Yao et al. 2023). Inhibition of ferroptosis more effectively suppresses primary retinal pigment epithelium cell death in the age-related macular degeneration model (Sun et al. 2018). Sestrin2 attenuates diabetic retinopathy by modulating ferroptosis through inhibiting phosphorylation of STAT3 and endoplasmic reticulum stress (Xi et al. 2024). Moreover, the lens epithelial cells exhibit high sensitization to ferroptosis (Wei et al. 2021). Therefore, targeting ferroptosis may represent a novel potential direction to understand and treat cataract, but the exact mechanism by which ferroptosis regulates in the process of cataract remains largely elusive.

Kirsten rat sarcoma (KRAS), a small GTPase with two variants containing 188 and 189 amino acids is categorized to RAS family (Rathod et al. 2023). The compatibility of KRAS is altered when GTP attaches to it, leading to better KRAS contact with Raf, PI3K, and Ral-GDS thereby enhances cell survival and proliferation, indicating KRAS plays a critical role in modulating intracellular controlling and signalling proliferation (Zhao et al. 2023). The KRAS activation is linked to increase of glycolysis, fatty acid or nucleotide synthesis, and maintenance of the energy levels (Singh et al. 2018; Pupo et al. 2019). Currently, the investigation of KRAS mainly involves in the tumour conditions such as non-small cell lung cancer and colorectal cancer (Lim et al. 2023; Nusrat and Yaeger 2023). However, the additional specific functions of KRAS, and whether KRAS can affect ferroptosis in cataract remain unclear.

Herein, ferroptosis-related differentially expressed genes (DEGs) and pivot genes were determined by the comprehensive bioinformatics analysis. We then attempted to unveil the functions of KRAS and underlying action mechanism on cataract, which may help improve the understanding of the complex pathogenesis for cataract and expect to reveal more potential targets regarding the management of cataract.

Materials and Methods

Data sources and identification of DEGs

The GSE3040 microarray data taken "cataract" as the keyword was downloaded from the Gene Expression Omnibus (GEO) database (https://www.ncbi.nlm.nih.gov/geo/), and further ferroptosis-related genes were screened. There were 3 normal human lens epithelial cells (LECs) samples (Control) and 3 human LECs samples (Cataract) treated with dexamethasone in the GSE3040. The GEO2R (www.ncbi.nlm.nih.gov/geo/geo2r) online tool was utilized to identify DEGs based on the thresholds of $p < 0.05$ and $|\log FC| > 2$. The volcano plot and heatmap were drawn to better visualize these DEGs, and the box plot was used for normalizing the data. Finally, a Venn diagram was depicted to screen intersection of the DEGs between GSE3040 dataset and ferroptosis-related genes through the EVenn tool (http://www.ehbio.com/test/venn/#/).

Functional enrichment analysis of overlapping DEGs

The Database for annotation, visualization and integrated discovery (DAVID) was applied to perform Gene Ontology (GO) annotation and Kyoto Encyclopedia of Genes and Genome (KEGG) pathway enrichment analysis. The enrichment analysis results were visualized in the bar graphs and bubble plots using "ggplot2 package" R software with $p < 0.05$ regarded as cut-off of enrichment significance.

PPI network construction and determination of the hub genes

The protein-protein interaction (PPI) network of the intersected DEGs was constructed through the Search Tool for the Retrieval of Interacting Genes (STRING, https://www.string-db.org) with a confidence interaction score 0.15 as the threshold condition. CytoHubba of Cytoscape software (version 0.1) was applied for screening the focal genes in the PPI network and calculating by the degree algorithm with the connectivity degree ≥ 0.

Analysis of hub genes

The principal component analysis (PCA) was carried out with the expression of hub genes in the original sample data as the variable, and the ridgeline plot was generated.

The GO enrichment chord diagram was plotted to assess the relationship between hub genes and potential pathways. In addition, the co-expressed genes of cataract and identified KRAS gene were screened through GeneCards and Coxpresdb database, followed by KEGG pathway enrichment analysis.

Cell culture and transfection

The SRA01/04 cells were purchased from iCell (Shanghai, China), then were cultured in DMEM medium (Hyclone, Logan, UT, USA) supplemented with 10% heat-inactivated fetal bovine serum (FBS, Hyclone), 100 U/ml penicillin and 100 μg/ml streptomycin (Hyclon) in a 5% CO_2 incubator at 37°C. For mimic cataract cell model *in vitro*, SRA01/04 cells

were treated with 50 μM fresh H_2O_2 media that was replaced every 3 days over a 2-week period.

KRAS knockdown in SRA01/04 cells was achieved by transfected with KRAS siRNA using Lipofectamine 2000 (Invitrogen, Cat. no. 11668019, California, USA). In addition, SRA01/04 cells in the H_2O_2-treated plus KRAS siRNA-transfected group were treated with 10 μM erastin for 24 h. The sequences of KRAS siRNAs, corresponding negative controls were designed by GenePharma (Shanghai, China) and were provided in Table S1 in Supplementary material.

Quantitative reverse-transcription polymerase chain reaction (qRT-PCR)

Total RNA was isolated using Trizol reagent (Invitrogen, Carlsbad, CA, USA) and PrimeScript RT Reagent kit (TaKaRa, Otsu, Japan) was adopted to synthesize cDNA. Afterwards, qRT-PCR was carried out on the ABI7500 quantitative PCR instrument (Thermo Fisher Scientific, Waltham, MA, USA) following the thermocycler conditions: 95°C for 30 s, followed by 40 cycles of 95°C for 10 s and 60°C for 30 s. The mRNA expression level was normalized with GAPDH as the internal standard using the $2^{-\Delta\Delta Ct}$ method. Gene-specific primers used for qRT-PCR were synthesized by Shenggong Bioengineering Company (Shanghai, China) and detailed in Table S1.

Western blot analysis

The total protein was extracted, harvested, quantified, separated, then shifted to the polyvinylidene difluoride membranes. After blocking with 5% non-fat milk, the membranes were subsequently rinsed with primary antibodies against COX2 (ab179800, 1:1000, Abcam, Cambridge, UK), GPX4 (ab125066, 1:5000, Abcam), YAP1 (ab205270,

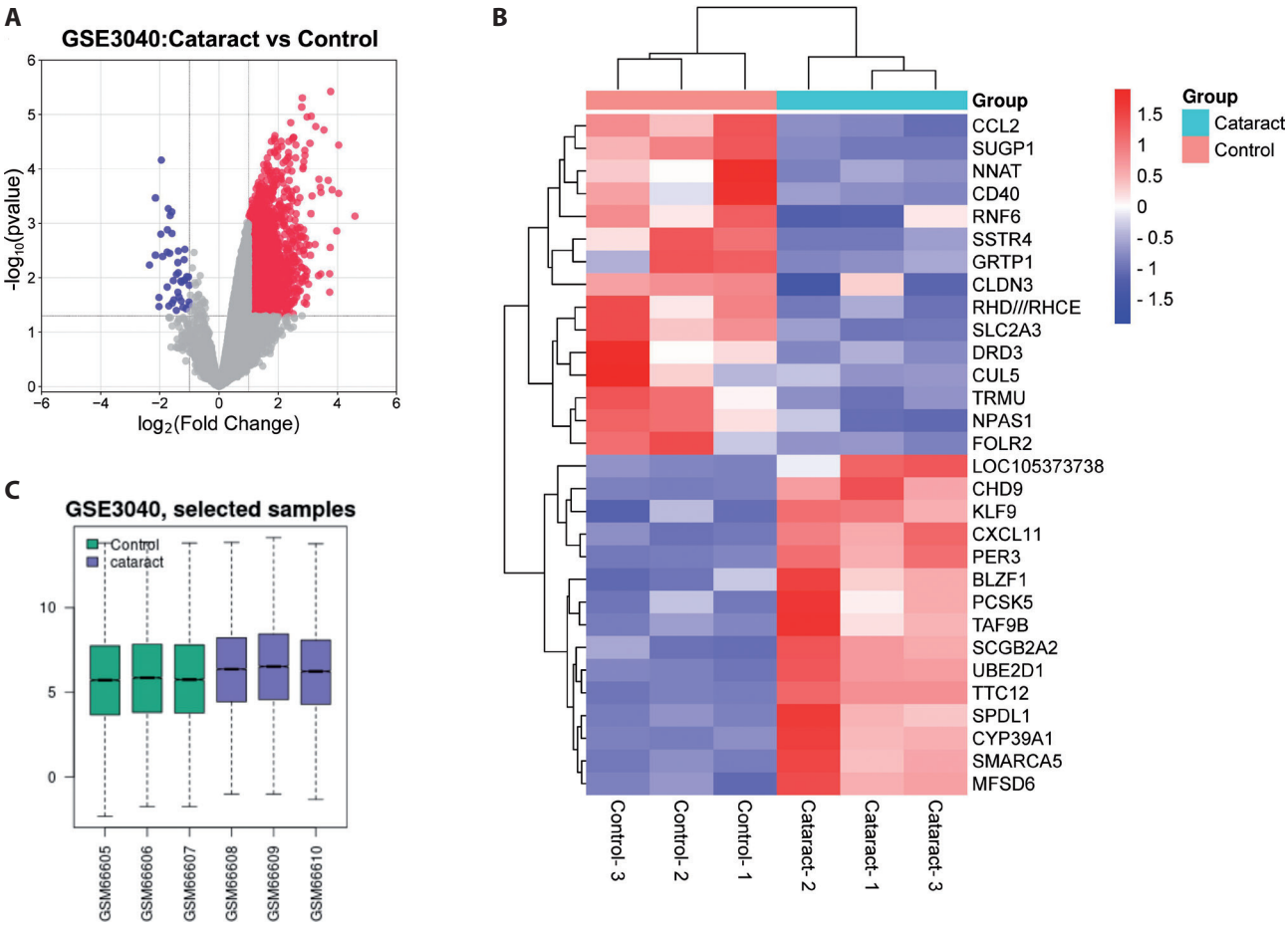

Figure 1. Identification of DEGs. **A.** Volcano plot of the 2428 DEGs in the GSE3040. Red, up-regulation. Blue, down-regulation. **B.** The DEGs' heat map. The sample numbers are located in the abscissa, while the gene names are in the ordinate. The upregulated DEGs are displayed by red, and the downregulated by blue. **C.** Box plot shows gene expression of each sample in GSE3040 dataset. Control, normal human lens epithelial cells; Cataract, human LECs samples treated with dexamethasone in the GSE3040. (For colour figure see online version of the article).

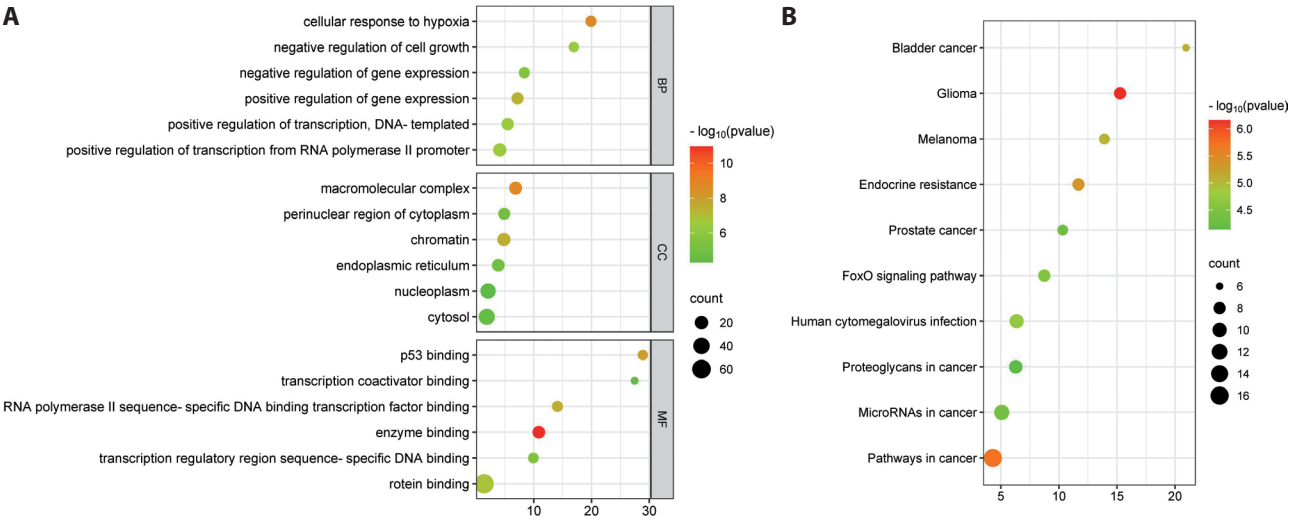

Figure 2. Analysis of the functional features of common DEGs. **A.** Gene Ontology (GO) functional analysis bubble plot. Top 6 GO enrichment terms in biological process (BP), cellular component (CC), and molecular function (MF) categories of the common DEGs, respectively. **B.** Kyoto Encyclopedia of Genes and Genome (KEGG) pathway analysis bubble plot. The first 10 KEGG enrichment pathways of common DEGs.

1:1000, Abcam), β-actin (4967S, 1:1000, Cell Signaling Technology, Danvers, MA, USA) at 4°C overnight. Next day, the membranes were labeled with the secondary antibody (Beyotime, Shanghai, China), and the immuno-reactive bands were detected using enhanced chemiluminescence kit (20148, Thermo Fisher, Shanghai, China) with β-actin as the loading control. The ImageJ software (V1.8.0.112, NIH, Madison, WI, USA) was applied for quantification of band intensity.

Cell viability assay

For the cell viability assay, the cells at the density of 1×10^4/well were grown in 96-well plates for 24 h. Then, 10 µl of diluted CCK-8 regents were supplemented to each well for an additional 2 h incubation. Finally, the absorbance of all plates was evaluated at 450 nm every hour on a microplate reader (VL0000D0, Thermo Fisher Scientific, Waltham, MA, USA).

EdU proliferation assay

Briefly, cells were seeded in 24-well plates at the density of 1×10^5/well until the cells reached 70–80% confluence and then labeled with 20 µM of 5-ethynyl-2'-deoxyuridine (EdU) working solution (Beyotime). Thereafter, the labelled cells were fixed with 4% paraformaldehyde, permeabilized in 0.1% Triton X-100 and dyed of nuclei with 4',6-diamidino-2-phenylindole (DAPI) solution. Finally, the stained cells were captured by microscopy (IX71, Olympus, Tokyo, Japan).

Measurement of cellular malondialdehyde, GSH and iron content

Briefly, the cellular supernatant was harvested from SRA01/04 cells in different treatment groups, then underwent centrifugation and resulting supernatant was removed to new centrifuge tubes for subsequent detection. The methods of activities assay of intracellular malondialdehyde (MDA), glutathione (GSH) levels, iron content, were determined using Malondialdehyde assay kit (S0131, Beyotime), total Glutathione Assay Kit (S0052, Beyotime) and Iron Assay Kit (ab83366, Abcam).

Statistical analysis

GraphPad Prism software 8.0 (GraphPad, San Diego, CA, USA) was applied for summarizing and statistically analyzing the results of all data with reported as mean value ± standard deviation (SD) of five independent experiments. Student's *t*-test was utilized to verify differences between two sets of data while one-way ANOVA was used for significance across multiple groups followed by Tukey's test. $p < 0.05$ was deemed as a statistically significant difference.

Results

Identification of DEGs

A total of 2428 DEGs were identified through the gene expression profile data GSE3040 with 2388 up-regulated and

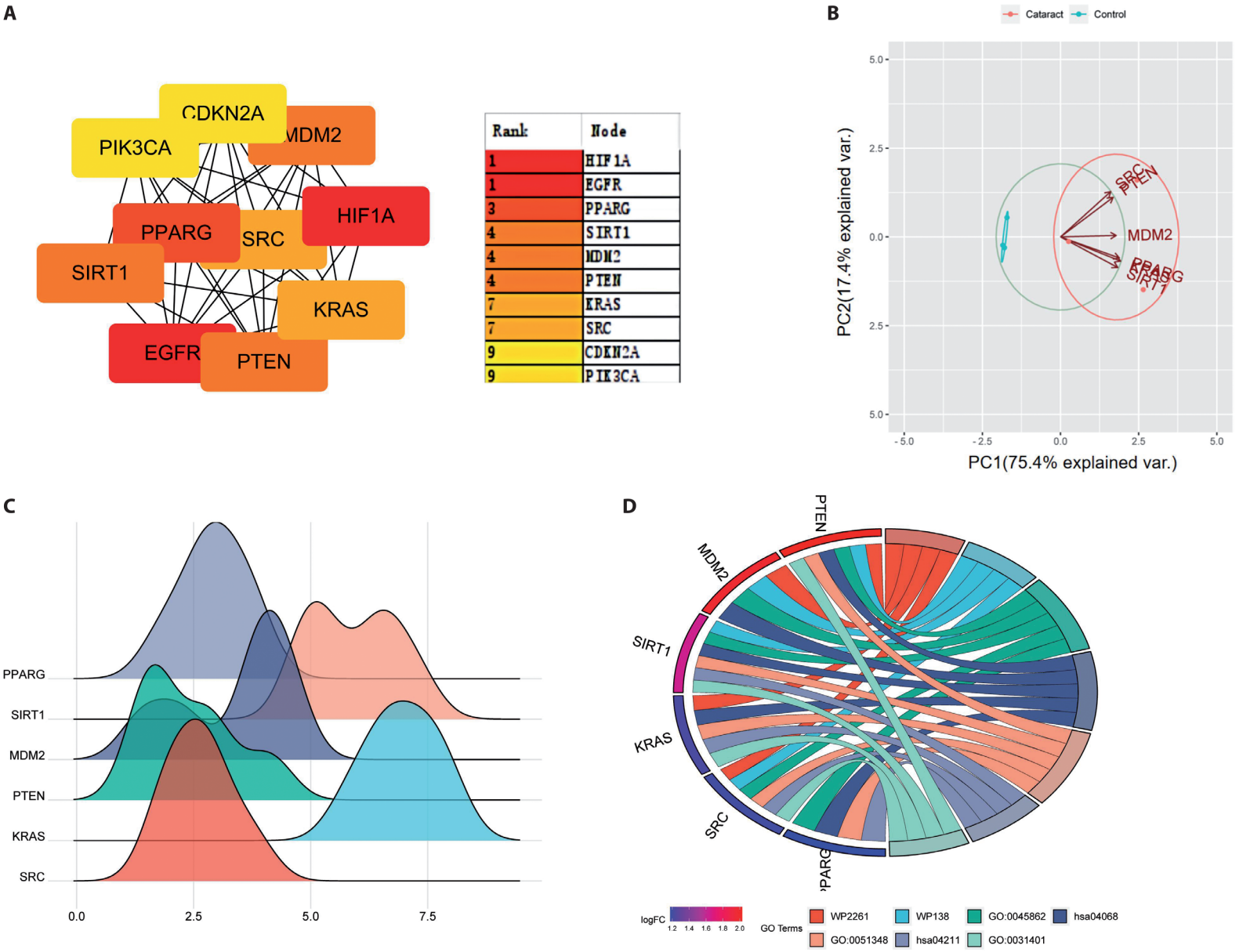

Figure 3. Identification of hub genes. **A.** The top 10 hub genes were calculated by degree in Cytoscape. The deeper the red node, the higher the degree of connectivity. **B.** Principal component analysis (PCA) analysis of hub genes. **C.** Ridgeline plots of hub genes. **D.** Chord diagram of GO enrichment analysis.

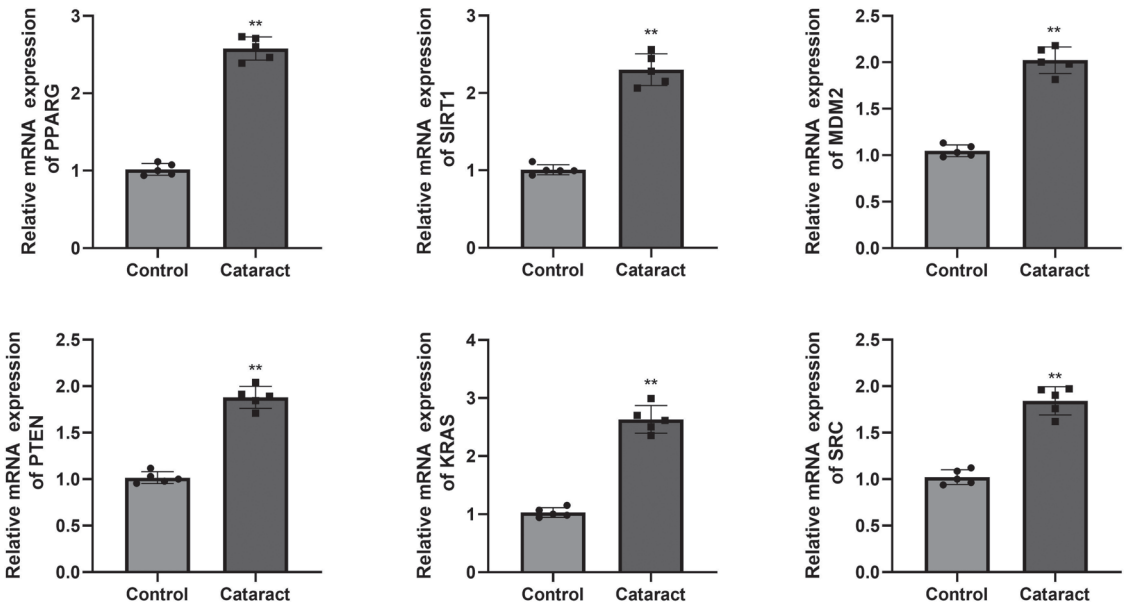

Figure 4. Quantification of hub genes using qRT-PCR. The expression levels of PPARG, SIRT1, MDM2, PTEN, KRAS and SRC were significantly increased in Cataract group. ** $p < 0.01$ *vs.* Control. Control, normal human lens epithelial cells; Cataract, human LECs samples treated with hydrogen peroxide (H_2O_2).

40 down-regulated genes, which was displayed in the corresponding volcano map (Fig. 1A). The top 15 significantly upregulated and downregulated DEGs were represented by heatmap (Fig. 1B). The standardization of gene expression in each sample of GSE3040 dataset was evaluated in the box plot (Fig. 1C). By cross analysing with ferroptosis-related genes, 73 common DEGs (co-DEGs) were obtained (Fig. S1 in Supplementary material).

Analysis of the functional features of common DEGs

In order to figure out the role of 73 co-DEGs, the GO and KEGG analysis were carried out. The top 6 results of the GO analysis met the criteria with the lowest *p* value were shown under each item of biological process (BP) including cellular response to hypoxia, negative regulation of cell growth, cell composition (CC) such as macromolecular complex, perinuclear region of cytoplasm as well as molecular function (MF) like P53 binding (Fig. 2A, Table S2). The KEGG pathway analysis showed the top 10 pathways with the lowest *p* value such as FOXO signalling way (Fig. 2B, Table S3).

Construction of PPI network and hub genes analysis

A construction of the PPI network was built using the STRING network analysis tool (Fig. S2). With the degree algorithm of plug-in CytoHubba, the top 10 ranking pivot genes were presented (Fig. 3A). Then the PCA analysis was carried out with two principal components (PC1 and PC2) effectively explained 92.8%, suggesting PC1 and PC2 effectiveness and could significantly distinguish Cataract from normal individuals (Fig. 3B). The ridgeline plots of hub genes in GSE3040 dataset showed that the distribution was relatively dense for PPARG, SIRT1, MDM2, PTEN, KRAS and SRC gene (Fig. 3C). Additionally, the GO enrichment chord diagram displayed there was a strong correlation among the six genes (Fig. 3D).

Quantification of hub genes

To further verify the expression of hub genes, the qRT-PCR experiment was carried out in cataract and control cells. The expression levels of PPARG, SIRT1, MDM2, PTEN, KRAS and SRC were significantly elevated in cataract group compared with control group (Fig. 4).

Downregulation of KRAS affects ferroptosis in cataract cell model

To evaluate the effect of KRAS on cataract, KRAS was silenced in SRA01/04 cells, and the expression of KRAS was downregulated in the SRA01/04 cells, and the si-KRAS-2 was selected for further experiments owing to transfection of si-KRAS-2 in the SRA01/04 cells with lowest expression (Fig. 5A). Erastin as ferroptosis inducer was employed to investigate the role of ferroptosis in the function of KRAS knockdown. The cell viability, proliferation of SRA01/04 cells treated with H_2O_2 were reduced, and this trend was

further decreased by erastin treatment, while KRAS silencing partially restored the inhibitory effects, indicating knockdown of KRAS could affect ferroptosis in cataract cell model (Fig. 5B,C).

Suppression of KRAS inhibits ferroptosis in H_2O_2-treated SRA01/04 cells

To further explore KRAS potential in ferroptosis regulation, the ferroptosis markers including COX2 and GPX4 protein expression were examined. The upregulated COX2 and downregulated GPX4 expression were observed in the H_2O_2-treated SRA01/04 cells, and this trend was further enhanced by erastin treatment, while was partially inhibited by KRAS depletion (Fig. 6A). Subsequently, we detected the content of GSH, MDA and iron. The levels of GSH were decreased, and MDA, iron content were elevated, and this tendency was aggravated after erastin treatment. KRAS knockdown had a limited influence on MDA and Fe^{2+} accumulation, and GSH reduction (Fig. 6B). Taken together, these findings indicated that KRAS silencing could suppress ferroptosis in H_2O_2-treated SRA01/04 cells.

Knockdown of KRAS can affect Hippo pathway in the cataract cell model

In order to further unravel the potential signaling pathway of KRAS gene involved in the development of cataract, we screened the co-expressed genes between genes related to cataract and KRAS gene through GeneCards and Coxpresdb database, and 337 genes were discovered (Fig. 7A). The KEGG enrichment revealed that these genes were partici-

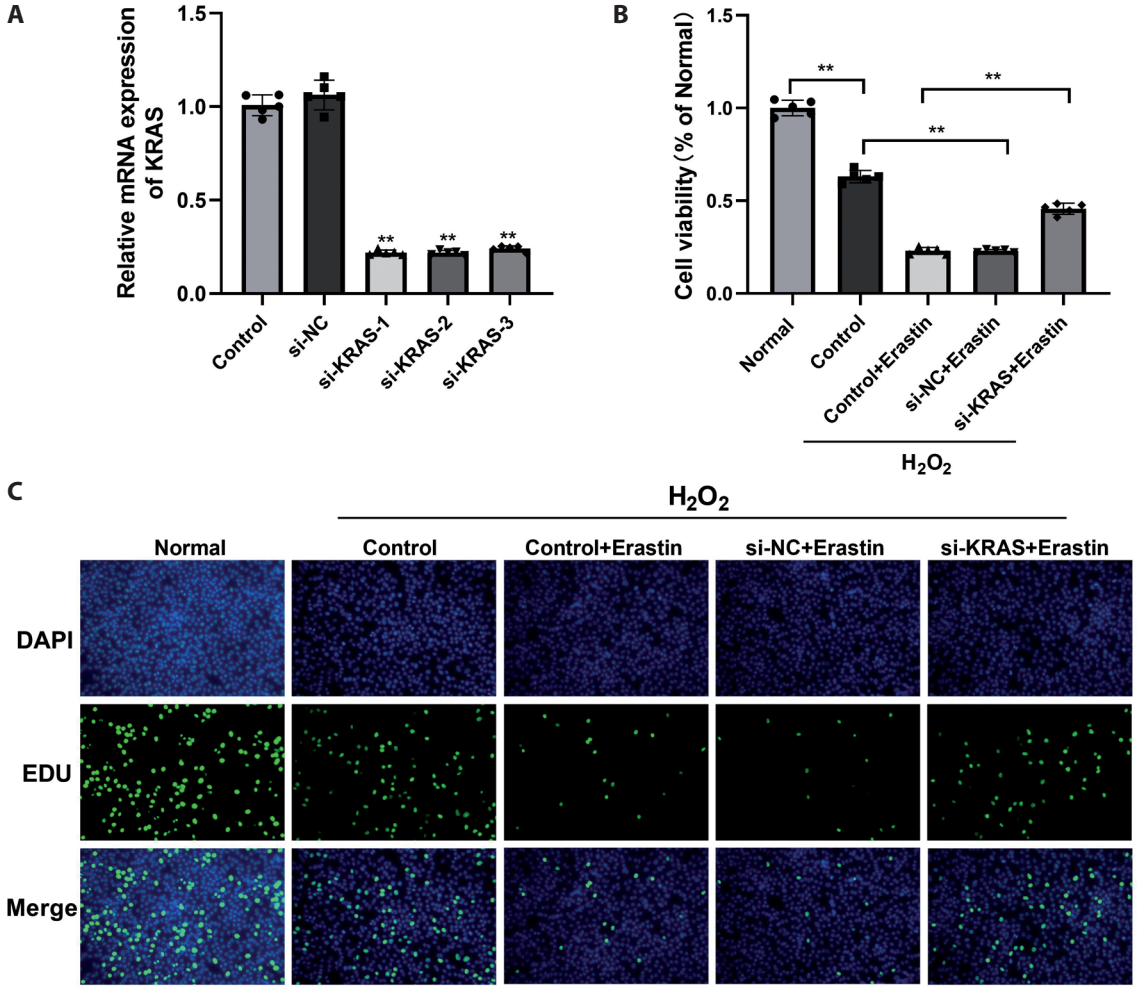

Figure 5. Downregulation of KRAS affects ferroptosis in cataract cell model. **A.** QRT-PCR assay was used to verify the knockdown efficiency of KRAS expression. **B.** Viability of SRA01/04 cells after different treatment using the CCK8 assay. **C.** Proliferation of SRA01/04 cells after different treatment using the 5-ethynyl-2'-deoxyuridine (EdU) assay. Green indicates EdU-incorporated cells, blue indicates nuclear staining with 4',6-diamidino-2-phenylindole (DAPI). ** $p < 0.01$.

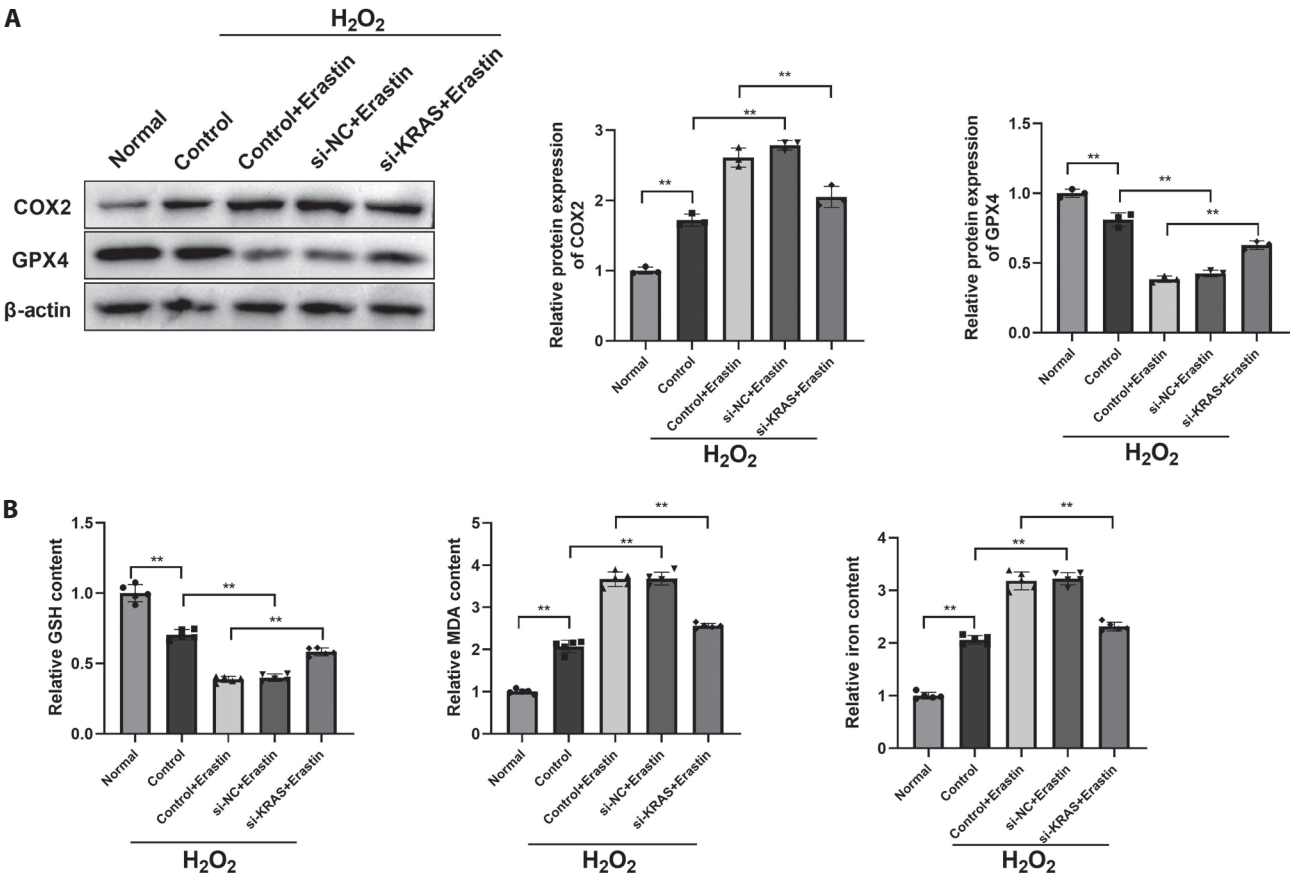

Figure 6. Suppression of KRAS inhibits ferroptosis in H_2O_2-treated SRA01/04 cells. **A.** Expression of COX2 and GPX4 in each group were detected by Western blot. **B.** The content of GSH, MDA and iron in SRA01/04 cells from each group were determined. ** $p < 0.01$.

pated in the Hippo signaling pathway (Fig. 7B). Afterwards, we examined the key protein expression related to the Hippo signaling pathway including YAP1. The expression level of YAP1 was decreased in the H_2O_2-treated SRA01/04 cells, and KRAS suppression led to the increase of YAP1 (Fig. 7C). Collectively, these data implied that deletion of KRAS may affect Hippo signaling pathway in cataract.

Discussion

Cataract is manifested as the opacification of the lens with rapidly increasing of the prevalence as the population aging that has become an internationally huge health burden (Xu et al. 2020; Ang and Afshari 2021; Falkowska et al. 2023). Further work is in requirement to explore the molecular mechanisms involved in the pathogenesis of cataract, which will greatly help find more novel therapeutic targets for cataract. Herein, we discovered 73 ferroptosis-associated genes through the comprehensive bioinformatics methods, and then the top 10 ranking pivot genes were identified by construction of PPI network. In addition, downregulation of KRAS was able to affect ferroptosis and Hippo signaling pathway in cataract cell model.

Among these genes, PPARG is identified as a risk factor for glucocorticoid-induced cataract through construction of ceRNA network (Shi et al. 2022). SIRT1 negatively regulates TXNIP/NLRP3 inflammasome pathway, which in turn enhances high glucose-induced inflammation and human LECs pyroptosis (Lian et al. 2023). MDM2 phosphorylation may result in LECs dealt with H_2O_2 apoptosis and age-related-cataract (Wang et al. 2020). PTEN can directly regulate lens ion transport through modulation of Na^+/K^+-ATPase activity dependent on AKT (Sellitto et al. 2013). In addition, the c-SRC kinase activation in LECs is along with increase of cell proliferation, mobility and migration (Li et al. 2019). In this study, the expression of PPARG, SIRT1, MDM2, PTEN, KRAS and SRC were elevated in cataract cell model, whereas the elaborate mechanisms behind these genes in cataract progression are worthy being further elucidated.

Of important, KRAS is elevated in gastric cancer stem-like cells, and blocking KRAS markedly attenuates gastric

tumorigenesis and metastasis (Yoon et al. 2023). KRAS depletion leads to the decrease of cell proliferation index in primary thyroid cancer cells (Liu et al. 2019). Suppression of KRAS reduces the proliferation rate in SW480 colorectal cancer cell line (Kamran et al. 2022). KRAS silencing significantly exhibits anti-proliferative effects in lung and colon adenocarcinoma cell lines (Pecot et al. 2014). In the present study, KRAS was upregulated in cataract group, and deletion of KRAS attenuated the inhibitory effects of viability and proliferation in H_2O_2-treated SRA01/04 cells plus erastin treatment.

Targeting ferroptosis provides therapeutic potentials for treatment of ocular diseases. For instance, ferroptosis induced by excessive oxidative stress is linked to the pathogenesis of dry eye disease, and AKR1C1 knock down decreases cell viability accompanied by increase of lipid peroxidation (Zuo et al. 2022). Phospholipase D silencing suppresses ferroptosis, as evidenced by reduction of reactive oxygen species, MDA, and increase of superoxide dismutase and glutathione in the retinal pigment epithelial cells (Park et al. 2023). HMOX1 increases the sensibility of human LECs to erastin, and knock-out or silencing of HMOX1 significantly improves the cell viability of human LECs under erastin treatment (Liao et al. 2023). Our findings demonstrated that ferroptosis was activated in the cataract cell model. Moreover, we linked our findings regarding KRAS silencing to ferroptosis, and revealed that KRAS knockdown retrained ferroptosis, as reflected by a limited influence on MDA and Fe^{2+} accumulation, GSH consumption, related ferroptosis hallmarks protein expression in the H_2O_2-treated SRA01/04 cells.

Hippo pathway is participated in the regulation of ocular development, and YAP is ubiquitously distributed in several ocular tissues (Fu et al. 2022), thus targeting Hippo components may present potential therapies for ocular diseases. It is observed that P-YAP expression is reduced in the photoreceptor layers of eyes from diabetic retinopathy rat model (Hao et al. 2017). The Hippo pathway-mediated regulation of the transcription cofactor YAP represents a fundamental regulatory mechanism that often prevents mammalian

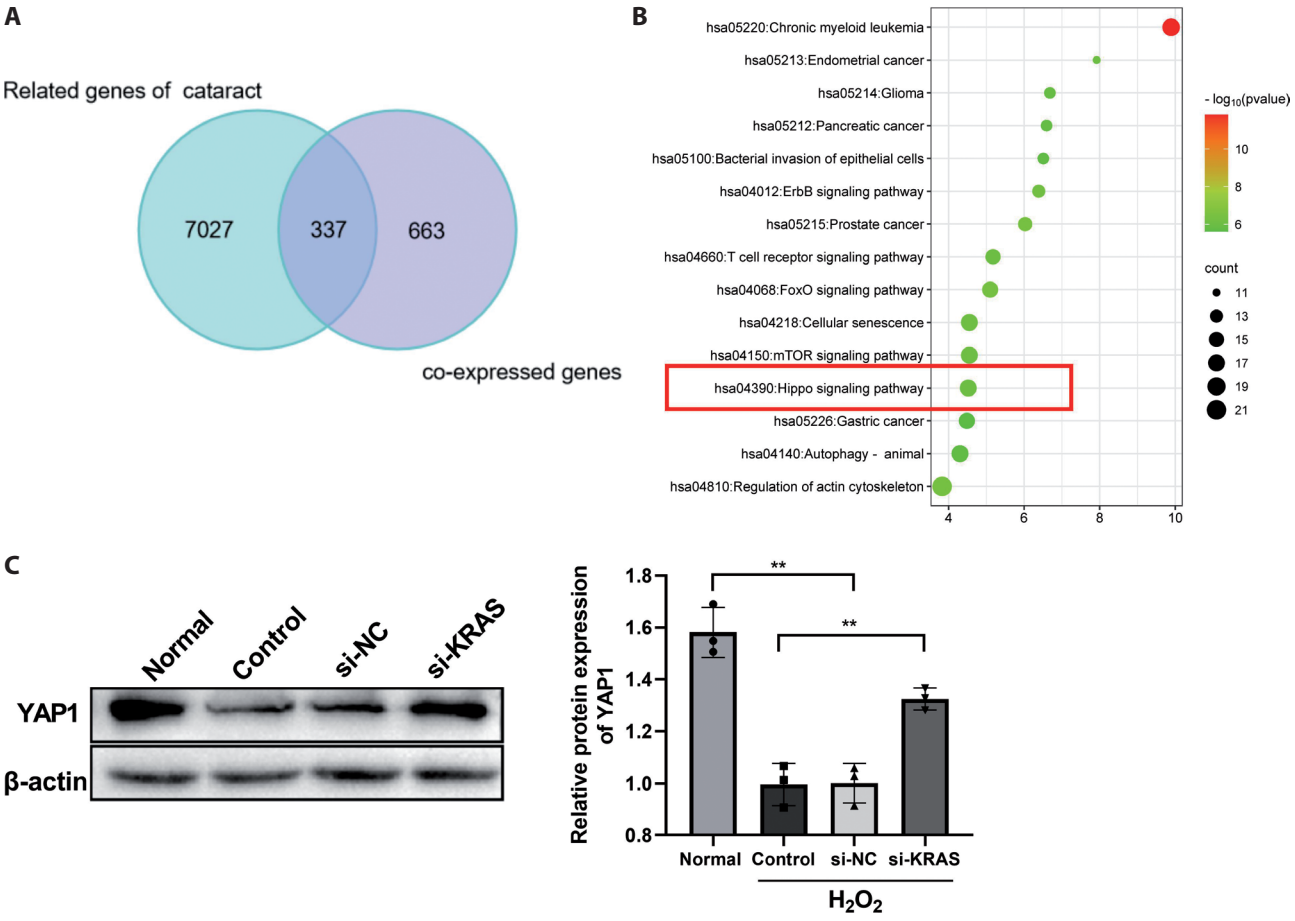

Figure 7. Knockdown of KRAS can affect HIPPO signaling pathway in the cataract cell model. **A.** Venn diagram of the co-expressed genes between genes related to cataract and KRAS gene. **B.** KEGG pathway analysis bubble plot. **C.** The expression level of the protein for YAP1 in each group were detected by Western blot. ** $p < 0.01$.

Müller glial cells proliferation (Rueda et al. 2019). Agrin can facilitate Yap1 dephosphorylation, thereby promoting proliferation of limbal stem cells and accelerating the corneal epithelium wound healing (Hou et al. 2020). Sestrin2 negatively modulates of YAP expression, and the proliferative capacity of corneal epithelial cells (Lee et al. 2020). Herein, our data revealed YAP1 expression was decreased in the H_2O_2-treated SRA01/04 cells, and KRAS deletion elevated YAP1 expression, indicating KRAS deletion is involved in the Hippo pathway activation.

To summarize, 73 ferroptosis-related DEGs, 10 hub genes were discovered through the comprehensive bioinformatics methods, among of which 6 core genes were confirmed upregulation in cataract cell model and may play pivotal roles in regulating cataract. Additionally, we elucidated that downregulation of KRAS exerted a suppressive role of ferroptosis, and could also affect Hippo pathway in cataract. Collectively, findings of this study not only provide profound insights into the novel functions of KRAS, but also may offer potential perspective makers targeting ferroptosis for cataract therapy.

Funding. Southwest Medical University research project, 2020ZRQNA040; Doctoral research Foundation of the Affiliated Hospital of Southwest Medical University, 20004.

Conflict of interest. The authors have no competing interests to declare that are relevant to the content of this article.

Author contributions. Hongda Jiang: substantial contributions to conception and design, data acquisition, drafting the article; Yinggui Yu and Yu Yan: data acquisition, reviewing the article. All the authors took part in the experiments. All the authors read and approved the manuscript.

References

Ang MJ, Afshari NA (2021): Cataract and systemic disease: A review. Clin. Exp. Ophthalmol. **49,** 118-127 https://doi.org/10.1111/ceo.13892

GBD 2019 Blindness and Vision Impairment Collaborators (2021): Causes of blindness and vision impairment in 2020 and trends over 30 years, and prevalence of avoidable blindness in relation to VISION 2020: the Right to Sight: an analysis for the Global Burden of Disease Study. Lancet Glob. Health **9,** e144-e160

Falkowska M, Mlynarczyk M, Micun Z, Konopinska J, Socha K (2023): Influence of diet, dietary products and vitamins on age-related cataract incidence: A systematic review. Nutrients **15,** 4585 https://doi.org/10.3390/nu15214585

Fu M, Hu Y, Lan T, Guan KL, Luo T, Luo M (2022): The Hippo signalling pathway and its implications in human health and diseases. Signal. Transduct. Target Ther. **7,** 376 https://doi.org/10.1038/s41392-022-01191-9

Hao GM, Lv TT, Wu Y, Wang HL, Xing W, Wang Y, Li C, Zhang ZJ, Wang ZL, Wang W, Han J (2017): The Hippo signaling pathway: a potential therapeutic target is reversed by a Chinese patent drug in rats with diabetic retinopathy. BMC Complement. Altern. Med. **17,** 187 https://doi.org/10.1186/s12906-017-1678-3

Hou L, Fu W, Liu Y, Wang Q, Wang L, Huang Y (2020): Agrin promotes limbal stem cell proliferation and corneal wound healing through hippo-yap signaling pathway. Invest. Ophthalmol. Vis. Sci. **61,** 7 https://doi.org/10.1167/iovs.61.5.7

Kamran S, Seyedrezazadeh E, Shanehbandi D, Asadi M, Zafari V, Shekari N, Namvar L, Zarredar H (2022): Combination therapy with KRAS and P38alpha siRNA suppresses colorectal cancer growth and development in SW480 cell line. J. Gastrointest. Cancer **53,** 597-604 https://doi.org/10.1007/s12029-021-00667-1

Kim R, Taylor D, Vonderheide RH, Gabrilovich DI (2023): Ferroptosis of immune cells in the tumor microenvironment.Trends Pharmacol. Sci. **44,** 542-552 https://doi.org/10.1016/j.tips.2023.06.005

Lapp T, Wacker K, Heinz C, Maier P, Eberwein P, Reinhard T (2023): Cataract surgery-indications, techniques, and intraocular lens selection. Dtsch. Arztebl. Int. **120,** 377-386 https://doi.org/10.3238/arztebl.m2023.0028

Lee JS, Park HW, Cho KJ, Lyu J (2020): Sestrin2 inhibits YAP activation and negatively regulates corneal epithelial cell proliferation. Exp. Mol. Med. **52,** 951-962 https://doi.org/10.1038/s12276-020-0446-5

Li X, Wang F, Ren M, Du M, Zhou J (2019): The effects of c-Src kinase on EMT signaling pathway in human lens epithelial cells associated with lens diseases. BMC Ophthalmol. **19,** 219 https://doi.org/10.1186/s12886-019-1229-4

Lian L, Le Z, Wang Z, Chen YA, Jiao X, Qi H, Hejtmancik JF, Ma X, Zheng Q, Ren Y (2023): SIRT1 inhibits high glucose-induced TXNIP/NLRP3 inflammasome activation and cataract formation. Invest. Ophthalmol. Vis. Sci. **64,** 16 https://doi.org/10.1167/iovs.64.3.16

Lian RR, Afshari NA (2020): The quest for homeopathic and non-surgical cataract treatment. Curr. Opin. Ophthalmol. **31,** 61-66 https://doi.org/10.1097/ICU.0000000000000631

Liao S, Huang M, Liao Y, Yuan C (2023): HMOX1 promotes ferroptosis induced by erastin in lens epithelial cell through modulates Fe(2+) production. Curr. Eye Res. **48,** 25-33 https://doi.org/10.1080/02713683.2022.2138450

Lim TKH, Skoulidis F, Kerr KM, Ahn MJ, Kapp JR, Soares FA, Yatabe Y (2023): KRAS G12C in advanced NSCLC: Prevalence, co-mutations, and testing. Lung Cancer **184,** 107293 https://doi.org/10.1016/j.lungcan.2023.107293

Liu A, Zhang W, Zhao T, Xiao M, Mei Q, Zhu H (2019): A single nuclear polymorphism in let-7g binding site affects the doubling time of thyroid nodule by regulating KRAS-induced cell proliferation. J. Cell. Physiol. **234,** 23437-23447 https://doi.org/10.1002/jcp.28912

Liu K, Li H, Wang F, Su Y (2023): Ferroptosis: mechanisms and advances in ocular diseases. Mol. Cell. Biochem. **478,** 2081-2095 https://doi.org/10.1007/s11010-022-04644-5

Liu YC, Wilkins M, Kim T, Malyugin B, Mehta JS (2017): Cataracts. Lancet **390,** 600-612 https://doi.org/10.1016/S0140-6736(17)30544-5

Nusrat M, Yaeger R (2023): KRAS inhibition in metastatic colorectal cancer: An update. Curr. Opin. Pharmacol. **68,** 102343 https://doi.org/10.1016/j.coph.2022.102343

Park SY, Kang HM, Park G, Oh JW, Choi YW (2023): OGD/R-induced ferroptosis and pyroptosis in retinal pigment epithelium cells: Role of PLD1 and PLD2 modulation. Cell. Biochem. Funct. **41,** 1162-1173 https://doi.org/10.1002/cbf.3848

Pecot CV, Wu SY, Bellister S, Filant J, Rupaimoole R, Hisamatsu T, Bhattacharya R, Maharaj A, Azam S, Rodriguez-Aguayo C, et al. (2014): Therapeutic silencing of KRAS using systemically delivered siRNAs. Mol. Cancer Ther. **13,** 2876-2885 https://doi.org/10.1158/1535-7163.MCT-14-0074

Pope LE, Dixon SJ (2023): Regulation of ferroptosis by lipid metabolism. Trends Cell. Biol. **33,** 1077-1087 https://doi.org/10.1016/j.tcb.2023.05.003

Pupo E, Avanzato D, Middonti E, Bussolino F, Lanzetti L (2019): KRAS-driven metabolic rewiring reveals novel actionable targets in cancer. Front. Oncol. **9,** 848 https://doi.org/10.3389/fonc.2019.00848

Rathod LS, Dabhade PS, Mokale SN (2023): Recent progress in targeting KRAS mutant cancers with covalent G12C-specific inhibitors. Drug Discov. Today **28,** 103557 https://doi.org/10.1016/j.drudis.2023.103557

Riaz Y, Mehta JS, Wormald R, Evans JR, Foster A, Ravilla T, Snellingen T (2006): Surgical interventions for age-related cataract. Cochrane Database Syst. Rev. **2006,** Cd001323 https://doi.org/10.1002/14651858.CD001323.pub2

Rueda EM, Hall BM, Hill MC, Swinton PG, Tong X, Martin JF, Poche RA (2019): The Hippo pathway blocks mammalian retinal muller glial cell reprogramming. Cell. Rep. **27,** 1637-1649.e6 https://doi.org/10.1016/j.celrep.2019.04.047

Sellitto C, Li L, Gao J, Robinson ML, Lin RZ, Mathias RT, White TW (2013): AKT activation promotes PTEN hamartoma tumor syndrome-associated cataract development. J. Clin. Invest. **123,** 5401-5409 https://doi.org/10.1172/JCI70437

Shi Z, Zhao X, Su Y, Wang C, Liu P, Ge H (2022): Screening of biological target molecules related to glucocorticoid-induced cataract (GIC) on the basis of constructing ceRNA network. Biochem. Genet. **60,** 24-38 https://doi.org/10.1007/s10528-021-10078-3

Singh A, Ruiz C, Bhalla K, Haley JA, Li QK, Acquaah-Mensah G, Montal E, Sudini KR, Skoulidis F, Wistuba, II, et al. (2018): De novo lipogenesis represents a therapeutic target in mutant Kras non- small cell lung cancer. FASEB J. **32,** 7018-7027 https://doi.org/10.1096/fj.201800204

Sun Y, Zheng Y, Wang C, Liu Y (2018): Glutathione depletion induces ferroptosis, autophagy, and premature cell senescence in retinal pigment epithelial cells. Cell Death Dis. **9,** 753 https://doi.org/10.1038/s41419-018-0794-4

Wang X, Zhou Y, Min J, Wang F (2023): Zooming in and out of ferroptosis in human disease. Front. Med. **17,** 173-206 https://doi.org/10.1007/s11684-023-0992-z

Wang Z, Su D, Sun Z, Liu S, Sun L, Li Q, Guan L, Liu Y, Ma X, Hu S (2020): MDM2 phosphorylation mediates H2O2-induced lens epithelial cells apoptosis and age-related cataract. Biochem. Biophys. Res. Commun. **528,** 112-119 https://doi.org/10.1016/j.bbrc.2020.05.060

Wei Z, Hao C, Huangfu J, Srinivasagan R, Zhang X, Fan X (2021): Aging lens epithelium is susceptible to ferroptosis. Free Radic. Biol. Med. **167,** 94-108 https://doi.org/10.1016/j.freeradbiomed.2021.02.010

Xi X, Chen Q, Ma J, Wang X, Zhang J, Li Y (2024): Sestrin2 ameliorates diabetic retinopathy by regulating autophagy and ferroptosis. J. Mol. Histol. **55,** 169-184 https://doi.org/10.1007/s10735-023-10180-3

Xu J, Fu Q, Chen X, Yao K (2020): Advances in pharmacotherapy of cataracts. Ann. Transl. Med. **8,** 1552 https://doi.org/10.21037/atm-20-1960

Yao F, Peng J, Zhang E, Ji D, Gao Z, Tang Y, Yao X, Xia X (2023): Pathologically high intraocular pressure disturbs normal iron homeostasis and leads to retinal ganglion cell ferroptosis in glaucoma. Cell Death Differ. **30,** 69-81 https://doi.org/10.1038/s41418-022-01046-4

Yoon C, Lu J, Jun Y, Suh YS, Kim BJ, Till JE, Kim JH, Keshavjee SH, Ryeom S, Yoon SS (2023): KRAS activation in gastric cancer stem-like cells promotes tumor angiogenesis and metastasis. BMC Cancer **23,** 690 https://doi.org/10.1186/s12885-023-11170-0

Zhao D, Liu Y, Yi F, Zhao X, Lu K (2023): Recent advances in the development of inhibitors targeting KRAS-G12C and its related pathways. Eur. J. Med. Chem. **259,** 115698 https://doi.org/10.1016/j.ejmech.2023.115698

Zuo X, Zeng H, Wang B, Yang X, He D, Wang L, Ouyang H, Yuan J (2022): AKR1C1 protects corneal epithelial cells against oxidative stress- mediated ferroptosis in dry eye. Invest. Ophthalmol. Vis. Sci. **63,** 3 https://doi.org/10.1167/iovs.63.10.3

Received: February 2, 2024
Final version accepted: March 12, 2024

doi: 10.4149/gpb_2024009

Supplementary Material

KRAS depletion suppresses ferroptosis and affects Hippo pathway in cataract

Hongda Jiang[1], Yinggui Yu[2] and Yu Yan[2]

[1] *Department of Laboratory Medicine, The Affiliated Hospital of Southwest Medical University, Luzhou City, Sichuan Province, China*
[2] *Department of Ophthalmology, The Affiliated Hospital of Southwest Medical University, Luzhou City, Sichuan Province, China*

Supplementary Tables

Table S1. Primer sequences

Name	Sequence (5'–3')
GAPDH-F	GAGTCAACGGATTTGGTCGT
GAPDH-R	TTGATTTTGGAGGGATCTCG
si-NC-F	UUCUCCGAACGUGUCACGUTT
si-NC-R	ACGUGACACGUUCGGAGAATT
si-KRAS-1-F	AUAUUCAGUCAUUUUCAGCAG
si-KRAS-1-R	GCUGAAAAUGACUGAAUAUAA
si-KRAS-2-F	UAUAUUCAGUCAUUUUCAGCA
si-KRAS-2-R	CUGAAAAUGACUGAAUAUAAA
si-KRAS-3-F	UUCUGAAUUAGCUGUAUCGUC
si-KRAS-3-R	CGAUACAGCUAAUUCAGAAUC
PPARG-F	GACCACTCCCACTCCTTTGA
PPARG-R	GATGCAGGCTCCACTTTGAT
SIRT1-F	TCAGTGGCTGGAACAGTGAG
SIRT1-R	TCTGGCATGTCCCACTATCA
MDM2-F	GGTGGGAGTGATCAAAAGGA
MDM2-R	GTGGCGTTTTCTTTGTCGTT
PTEN-F	GTTTACCGGCAGCATCAAAT
PTEN-R	CCCCCACTTTAGTGCACAGT
KRAS-F	CACGGTCATCCAGTGTTGTC
KRAS-R	CACCACCCCAAAATCTCAAC
SRC-F	CAGAGAGGGAAAGCCACTTG
SRC-R	GCTTGCTCTTGTTGCTACCC

F, forward; R, reverse.

Table S2. GO TERM analysis of common differentially expressed genes

GOTERM	Term	p value	Fold enrichment	Count	GeneRatio	Genes
GOTERM_BP_DIRECT	cellular response to hypoxia	1.56E-09	19.89572685	10	13.69863014	PRKAA1, EPAS1, SRC, PTEN, MDM2, MDM4, PPARG, HIF1A, SIRT1, PPARD
GOTERM_BP_DIRECT	positive regulation of gene expression	5.00E-08	7.191596062	14	19.17808219	ATF2, MEF2C, PRKAA1, CDKN2A, CAV1, ACVR1B, HIF1A, AR, GJA1, MDM2, KRAS, PPARG, TLR4, PPARD
GOTERM_BP_DIRECT	positive regulation of transcription from RNA polymerase II promoter	3.70E-07	4.111568226	19	26.02739726	RB1, ATF2, MEF2C, CDKN2A, EPAS1, NCOA3, HMGB1, HIF1A, SIRT1, EGFR, AR, NR4A1, NR5A2, TFR2, PPARG, LPIN1, TLR4, TP63, PPARD
GOTERM_BP_DIRECT	positive regulation of transcription, DNA-templated	3.83E-07	5.478138488	15	20.54794521	KDM5A, MEF2C, PRKAA1, CDKN2A, SRC, HIF1A, EGFR, MTDH, AR, NR5A2, TFAM, PPARG, BRD7, TP63, PPARD
GOTERM_BP_DIRECT	negative regulation of cell growth	4.19E-07	16.92715808	8	10.95890411	RB1, MEG3, GJA1, CDKN2A, PPARG, ACVR1B, SIRT1, PPARD
GOTERM_BP_DIRECT	negative regulation of gene expression	2.62E-06	8.357452656	10	13.69863014	RB1, MEF2C, GJA1, PRKAA1, PIK3CA, SRC, PPARG, ACVR1B, HIF1A, SIRT1
GOTERM_CC_DIRECT	macromolecular complex	1.86E-09	6.853608086	17	23.28767123	USP7, MEF2C, CDKN2A, NCOA3, CAV1, HIF1A, SIRT1, EGFR, PANX1, AR, SNX4, SCP2, PEX3, NEDD4, MDM2, TFAM, TP63
GOTERM_CC_DIRECT	chromatin	3.35E-08	4.826984088	19	26.02739726	RB1, KDM5A, ATF2, MEF2C, PRKAA1, EPAS1, NCOA3, HIF1A, SIRT1, AR, NR4A1, NR5A2, NEDD4, PPARG, BRD7, TP63, EZH2, BRDT, PPARD
GOTERM_CC_DIRECT	endoplasmic reticulum	1.04E-05	3.853803556	16	21.91780822	ELOVL5, YTHDC2, CAV1, ACSL4, PRKCA, ACSL3, HMGB1, MTDH, PANX1, GJA1, PGRMC1, SCP2, SCD, PEX3, NOX5, LPIN1
GOTERM_CC_DIRECT	perinuclear region of cytoplasm	1.05E-05	4.879546528	13	17.80821918	SRC, YTHDC2, CAV1, PRKCA, ACSL3, EGFR, MTDH, PIK3CA, NEDD4, LAMP2, PPARG, NF2, TLR4
GOTERM_CC_DIRECT	cytosol	3.31E-05	1.860278353	37	50.68493151	RB1, PRKAA1, EPAS1, SRC, IREB2, PTEN, ALOX12, ACVR1B, HIF1A, GJA1, SCP2, BRD7, OSBPL9, ATG3, USP7, MEF2C, PARP4, CDKN2A, NCOA3, IDH1, PRKCA, SIRT1, NR4A1, AR, GCLC, PIK3CA, NEDD4, AGPS, CCDC6, MDM2, TFAM, RBMS1, KRAS, PPARG, NF2, LPIN1, CHMP5
GOTERM_CC_DIRECT	nucleoplasm	4.82E-05	2.082514339	30	41.09589041	RB1, KDM5A, ATF2, PRKAA1, EPAS1, SRC, PTEN, HMGB1, HIF1A, GJA1, SCP2, BRD7, TP63, USP7, MEF2C, PARP4, CDKN2A, NCOA3, PRKCA, SIRT1, NR4A1, AR, NR5A2, PEX3, MDM2, PPARG, MDM4, LPIN1, PPARD, EZH2
GOTERM_MF_DIRECT	enzyme binding	1.13E-11	10.86827033	16	21.91780822	RB1, ATG3, PARP4, SRC, CAV1, PTEN, PRKCA, HIF1A, SIRT1, EGFR, AR, NEDD4, LAMP2, MDM2, MDM4, PPARG
GOTERM_MF_DIRECT	p53 binding	1.02E-08	28.88280061	8	10.95890411	USP7, CDKN2A, MDM2, MDM4, BRD7, HIF1A, SIRT1, TP63

(continued)

Table S2. (continued)

GOTERM	Term	p value	Fold enrichment	Count	GeneRatio	Genes
GOTERM_MF_DIRECT	RNA polymerase II sequence-specific DNA binding transcription factor binding	3.18E-08	14.09387998	10	13.69863014	RB1, ATF2, AR, MEF2C, EPAS1, CDKN2A, HMGB1, HIF1A, TRIB2, MTDH
GOTERM_MF_DIRECT	rotein binding	1.48E-07	1.395134884	67	91.78082192	RB1, KDM5A, ATF2, PTEN, HMGB1, SLC7A11, PANX1, GJA1, SCP2, LAMP2, TP63, ATG3, SLC38A1, USP7, MEF2C, PARP4, ELOVL5, MMD, NCOA3, PRKCA, ACSL3, SIRT1, AR, NR5A2, PIK3CA, PEX3, TFR2, AGPS, RBMS1, TFAM, PPARG, TRIB2, TLR4, DLD, CHMP5, PPARD, PRKAA1, SRC, EPAS1, YTHDC2, IREB2, ALOX12, ACVR1B, HIF1A, EGFR, MTDH, DPP4, SNX4, PGRMC1, ADAM23, BRD7, OSBPL9, SLC16A1, CDKN2A, IDH1, CAV1, NR4A1, GCLC, SCD, NEDD4, CCDC6, MDM2, KRAS, MDM4, NF2, LPIN1, EZH2
GOTERM_MF_DIRECT	transcription regulatory region sequence-specific DNA binding	3.03E-06	9.924686192	9	12.32876712	KDM5A, AR, MEF2C, NR5A2, TFAM, PPARG, HMGB1, BRD7, TP63
GOTERM_MF_DIRECT	transcription coactivator binding	3.09E-05	27.4537037	5	6.849315068	AR, EPAS1, TFAM, HIF1A, PPARD

Table S3. KEGG Pathway analysis of common differentially expressed genes

KEGG_PATHWAY	Term	p value	Fold enrichment	Count	GeneRatio	Genes
KEGG_PATHWAY	Glioma	6.93E-07	15.264	8	10.95890411	RB1, PIK3CA, CDKN2A, PTEN, MDM2, KRAS, PRKCA, EGFR
KEGG_PATHWAY	Pathways in cancer	1.92E-06	4.311864407	16	21.91780822	RB1, CDKN2A, EPAS1, NCOA3, PTEN, PRKCA, HIF1A, EGFR, AR, PIK3CA, MDM2, CCDC6, KRAS, PPARG, IFNA10, PPARD
KEGG_PATHWAY	Endocrine resistance	4.27E-06	11.68163265	8	10.95890411	RB1, PIK3CA, CDKN2A, SRC, NCOA3, MDM2, KRAS, EGFR
KEGG_PATHWAY	Bladder cancer	8.00E-06	20.94146341	6	8.219178082	RB1, CDKN2A, SRC, MDM2, KRAS, EGFR
KEGG_PATHWAY	Melanoma	8.93E-06	13.9125	7	9.589041096	RB1, PIK3CA, CDKN2A, PTEN, MDM2, KRAS, EGFR
KEGG_PATHWAY	Human cytomegalovirus infection	2.00E-05	6.36	10	13.69863014	RB1, ATF2, PIK3CA, CDKN2A, SRC, MDM2, KRAS, PRKCA, EGFR, IFNA10
KEGG_PATHWAY	FoxO signaling pathway	2.89E-05	8.738931298	8	10.95890411	USP7, PRKAA1, PIK3CA, PTEN, MDM2, KRAS, SIRT1, EGFR
KEGG_PATHWAY	MicroRNAs in cancer	4.25E-05	5.077741935	11	15.06849315	PIK3CA, CDKN2A, PTEN, MDM2, MDM4, KRAS, PRKCA, SIRT1, TP63, EGFR, EZH2
KEGG_PATHWAY	Prostate cancer	4.95E-05	10.32680412	7	9.589041096	RB1, AR, PIK3CA, PTEN, MDM2, KRAS, EGFR
KEGG_PATHWAY	Proteoglycans in cancer	7.18E-05	6.282439024	9	12.32876712	PIK3CA, SRC, CAV1, MDM2, KRAS, PRKCA, HIF1A, TLR4, EGFR

Supplementary Figures

Figure S1. Venn diagram of DEGs and ferroptosis-related genes

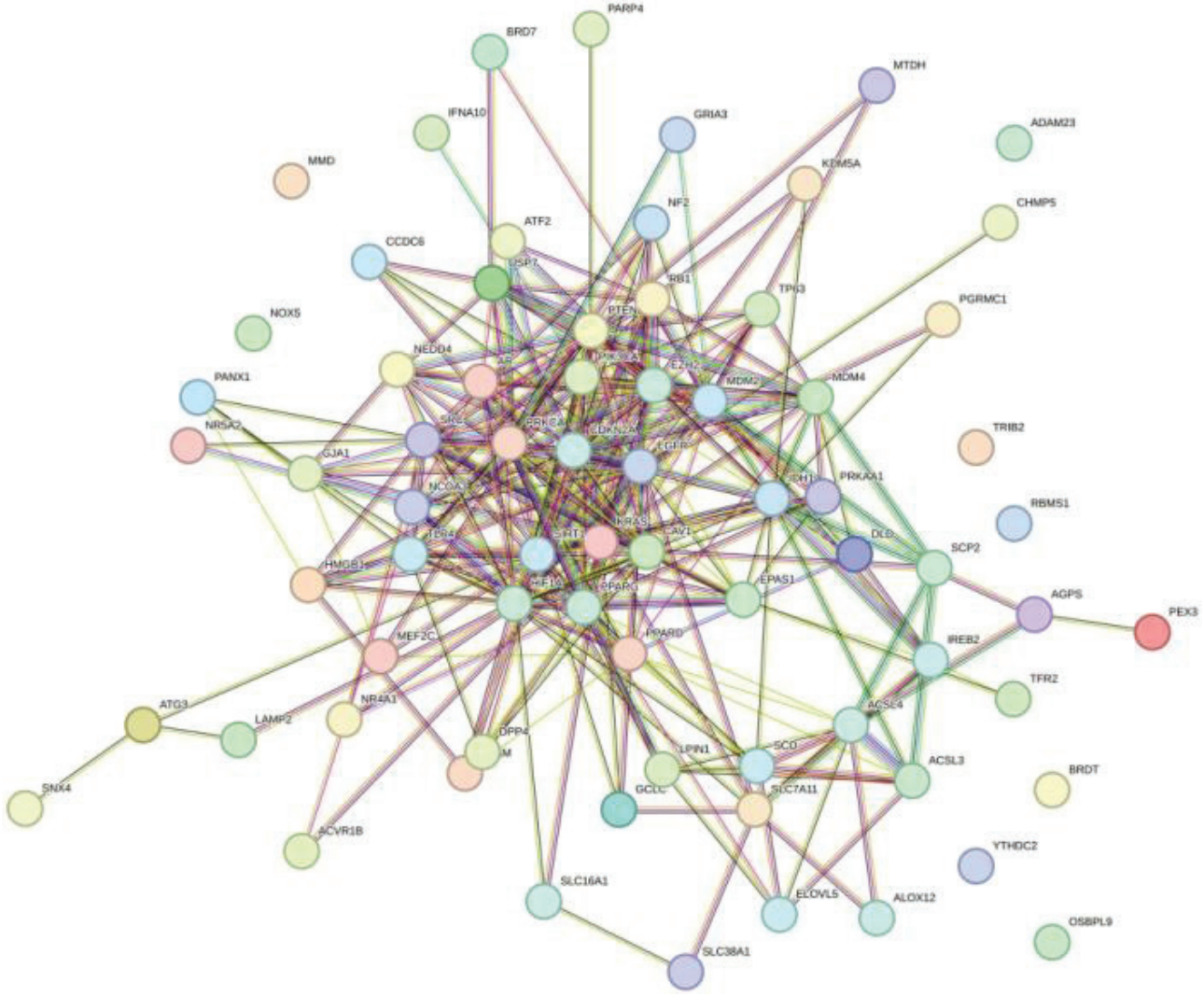

Figure S2. The protein-protein interaction (PPI) network of overlapping genes